

Using a Feedback-Based Quantum Algorithm to Analyze the Critical Properties of the ANNNI Model Without Classical Optimization

G. E. L. Peixe,^{1,*} L. A. M. Rattighieri,^{1,*} A. L. Malvezzi,¹ and F. F. Fanchini^{1,2,†}

¹*Faculty of Sciences, UNESP - São Paulo State University, 17033-360 Bauru-SP, Brazil*

²*QuaTI - Quantum Technology & Information, 13560-161 São Carlos-SP, Brazil*

(Dated: June 27, 2024)

We investigate the critical properties of the Anisotropic Next-Nearest-Neighbor Ising (ANNNI) model using a feedback-based quantum algorithm (FALQON). This approach allows us to compute both ground and excited states without relying on classical optimization methods. We study the quantum phase transitions using the Finite Size Scaling method, analyze correlation functions through spin correlations in the ground state, and examine magnetic structure by calculating structure factors via the Discrete Fourier Transform. Our results demonstrate the algorithm's capability to identify quantum phase transitions and efficiently map the ANNNI model's magnetic phases, establishing FALQON as a powerful tool to study complex magnetic systems.

I. INTRODUCTION

Calculating ground and excited states of Hamiltonians in many-body quantum systems is intrinsically related to elements of interest analyzed through quantum simulation algorithms. Algorithms that enable the acquisition of these states are a central focus of quantum simulation research [1–5]. Despite the inherent complexity of searching for generic ground states, even on quantum computers [6], recent advances in technology have ushered in the era of noisy intermediate-scale quantum (NISQ) computers [7]. This progress has driven substantial research into the application of NISQ devices, particularly in quantum simulation [8, 9], focusing on determining ground states of physical, chemical, and material systems using the Variational Quantum Eigensolver (VQE) Algorithm [10–12] and the Quantum Approximate Optimization Algorithm (QAOA) [13]. However, VQE and QAOA face a significant practical challenge, the need for classical optimization of quantum circuit parameters to minimize an objective function, a task that becomes increasingly complex as the search space dimension grows.

In this study, we explore an alternative approach that eliminates the need for optimization, thereby avoiding this complexity. Unlike classical optimization of a parameterized circuit, our proposed strategy utilizes a feedback law principle to sequentially establish quantum circuit parameter values, layer by layer, based on feedback from measurements of qubits in the preceding layer. This feedback principle is based on Lyapunov quantum control theory [14] and has been developed to ensure that the objective function value monotonically decreases with circuit depth. This approach represents an innovative application of Feedback-based Quantum Algorithms (FQAs), extending principles from the Feedback-based Quantum Optimization Algorithm (FALQON) [1, 15, 16], recently developed for combinatorial optimization. Our study

specifically focuses on the development of FALQON, exploring symmetries to achieve excited states. This approach enables a detailed investigation of the phase diagram, correlation functions, and structural factors associated with the one-dimensional Anisotropic Next-Nearest-Neighbor Ising (ANNNI) model.

Investigating the phase diagram of the ANNNI model is essential for understanding the magnetic behavior of matter at microscopic levels. This configuration provides significant understanding of the fundamental magnetic characteristics of the system. Once the ground state is known, spin correlation functions can be examined to show how spins at different positions in the lattice are related to each other. Another important aspect is the analysis of structural factors through the discrete Fourier transform, which allows us to study spin oscillation patterns at different wavelengths. This is crucial for understanding the spatial organization of magnetic moments and how magnetic oscillations propagate along a chain.

The structure of this article is organized as follows: Section II provides a detailed review of the ANNNI model Hamiltonian, discussing its construction and phase diagram. Section III offers an in-depth review of FALQON. The results of quantum simulations are presented in Section IV. Conclusions and future perspectives are discussed in Section V.

II. ANNNI MODEL

A. Hamiltonian

The ANNNI model is a fundamental theoretical model in statistical physics that describes the behavior of spins in a one-dimensional magnetic system. This model is particularly interesting due to its anisotropy in interactions between nearest and next-nearest neighbor spins [17, 18]. Here, we are interested in the stability of phases present in the model and the phase transitions driven by quantum fluctuations at zero temperature. Quantum fluctuations can be further influenced by the presence of a transverse

* These authors contributed equally to this work

† felipe.fanchini@unesp.br

field. Therefore, we consider the properties of the ground state of the ANNNI model in a transverse field at zero temperature. Frustration is expected to arise due to the presence of next-nearest neighbor interactions, leading to interesting quantum phases. The model can be described by the following Hamiltonian:

$$H_p = -J \sum_{j=1}^L (\sigma_j^z \sigma_{j+1}^z - \kappa \sigma_j^z \sigma_{j+2}^z + g \sigma_j^x), \quad (1)$$

where σ_j^a , with $a = x, y, z$, are the Pauli matrices acting on site j of a one-dimensional lattice (chain) with L sites. For a chain with L sites, the Hamiltonian H acts in a Hilbert space of dimension 2^L , which is the tensor product of L two-dimensional spaces. The coupling constant $J(> 0)$ represents the ferromagnetic interaction strength between nearest neighbors, defining the energy scale (we set $J = 1$), while $\kappa(> 0)$ and $g(> 0)$ are dimensionless coupling constants associated with next-nearest neighbor interactions and the transverse magnetic field, respectively.

B. Phase Diagram

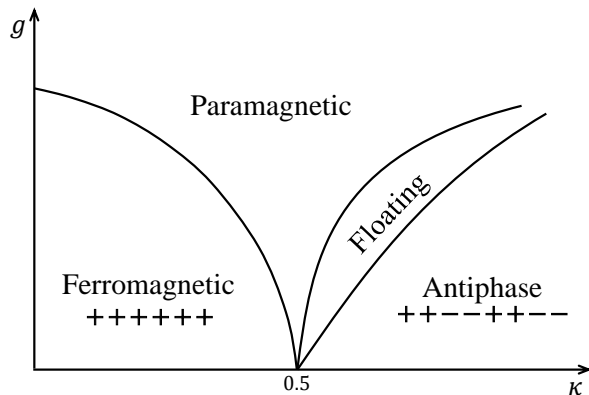


Figure 1. Schematic phase diagram of the transverse ANNNI model. [19]

The phase diagram of the ground state of the ANNNI model reveals four distinct phases: ferromagnetic, antiferromagnetic, paramagnetic, and incommensurate floating, each separated by three quantum phase transitions, as shown in Figure (1).

Understanding the phases of the ANNNI model is essential for comprehending its interactions [18, 20, 21]. Spins at different sites interact via coupling pairs $-J_{ij} S_i^z S_j^z$, where J_{ij} are exchange integrals. The spin arrangement is determined by the nature of these interactions. When $J_{ij} > 0$, spins prefer to align in the same

direction, whereas for $J_{ij} < 0$, they prefer opposite directions.

In the ANNNI model, nearest neighbors interact ferromagnetically ($J_1 = J > 0$), while second-nearest neighbors interact antiferromagnetically ($J_2 < 0$). When the interaction between nearest neighbors predominates, the system is in the ferromagnetic phase. However, when second-nearest neighbor interaction becomes significant, the system exhibits a staggered solution, leading to the antiphase [22]. Furthermore, the inclusion of a transverse field in the ANNNI model introduces a tendency towards disorder, resulting in the paramagnetic phase, where spins do not exhibit a characteristic alignment with respect to the z -direction.

III. FALQON: FEEDBACK-BASED ALGORITHM FOR QUANTUM OPTIMIZATION

In this section, we introduce the concept of Feedback-based Quantum Algorithms (FQAs) and their relationship with the continuous Lyapunov quantum control framework. This approach is aligned with the content presented by [15], who introduced FALQON as an FQA for solving combinatorial optimization problems. Additionally, we further develop FALQON to find ground and excited states of the ANNNI model. As proposed by Magann et al. in their manuscript, we begin with a quantum system whose dynamics are governed by

$$i \frac{d}{dt} |\psi(t)\rangle = (H_p + H_d \beta(t)) |\psi(t)\rangle. \quad (2)$$

The general solution of this equation is expressed as:

$$|\Psi(t)\rangle = \tau e^{-i \int_0^t (H_p + H_d \beta(t')) dt'} |\Psi(0)\rangle, \quad (3)$$

where τ denotes the time ordering operator, H_d is referred to as the control Hamiltonian, and $\beta(t)$ is a time-dependent control function. The goal of the numerical method is to infer a dynamic by adjusting $\beta(t)$ such that the resulting quantum state tends towards the ground state of H_p .

Before outlining the strategy to compute the appropriate function for $\beta(t)$, we will first demonstrate how to implement the aforementioned dynamics in a quantum circuit. For this purpose, we discretize the evolution into two steps. First, time is divided into a sequence of l steps, and the Hamiltonian is approximated as time-independent in each step:

$$|\Psi(t + \Delta t)\rangle = e^{-i(H_p + \beta(t)H_d)\Delta t} |\Psi(t)\rangle. \quad (4)$$

The second step involves approximating the evolution in each time step using trotterization. This sequence of approximations aims to decompose the complex unitary operation into a product of simpler exponentials:

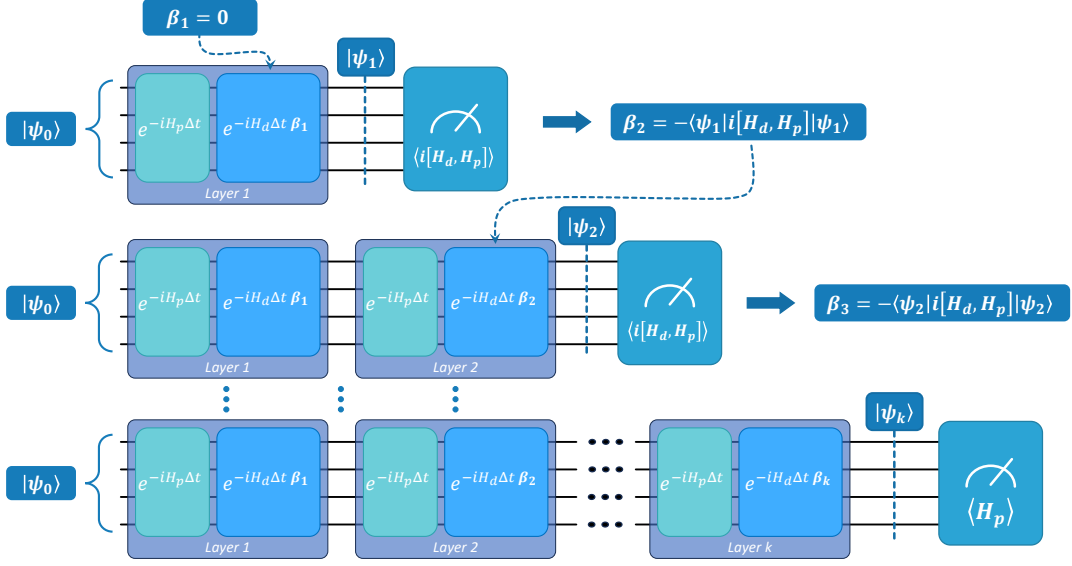


Figure 2. Illustrative diagram of the FALQON quantum algorithm. The process starts with an initial state $|\psi_0\rangle$. At each layer k , the unitary operators $e^{-iH_p\Delta t}$ and $e^{-iH_d\Delta t\beta_k}$ are sequentially applied to the current state, adaptively adjusting the parameter β_k . This process is iteratively repeated to approximate the target state, representing the evolution of the state $|\psi\rangle$ across the layers until reaching the desired solution.

$$|\Psi_l\rangle = e^{-i\beta_l H_d \Delta t} e^{-iH_p \Delta t} \dots e^{-i\beta_1 H_d \Delta t} e^{-iH_p \Delta t} |\Psi_0\rangle = U_d(\beta_l) U_p \dots U_d(\beta_1) U_p |\Psi_0\rangle, \quad (5)$$

representing the discretization of Eq. (3) into a form suitable for study on a quantum computer. Here, $\beta_k \equiv \beta(k\Delta t)$ with $k = 1, 2, \dots, l$, $|\Psi_k\rangle \equiv |\Psi(k\Delta t)\rangle$, $U_p \equiv e^{-iH_p \Delta t}$, and $U_d(\beta_k) \equiv e^{-i\beta_k H_d \Delta t}$. This provides us with a straightforward method to implement the desired dynamics on a quantum computer.

Given this approach, we will now consider an appropriate form for $\beta(t)$, a function that drives the initial state to the ground state of H_p . We seek $\beta(t)$ in a way that

$$\frac{d}{dt} \langle \psi(t) | H_p | \psi(t) \rangle (t) \leq 0, \quad \forall t \geq 0. \quad (6)$$

Indeed, there are various functions for $\beta(t)$ that can guide the quantum state to the ground state, and one possible choice is given by $\beta(t) = -i\langle \Psi(t) | [H_d, H_p] | \Psi(t) \rangle$ [15]. Given this, we can now describe the mechanics of implementing FALQON as illustrated in Figure (2). The first step is to select an initial state $|\Psi_0\rangle$ and a time step Δt , and start the algorithm with a value for β_1 . FQAs then use the feedback law:

$$\beta_k = -A_{k-1}, \quad (7)$$

where $A_k = i\langle \Psi_k | [H_d, H_p] | \Psi_k \rangle$, to determine the values of the quantum circuit parameters β_k at steps $k = 2, \dots, l$. The term in Eq. (7) is termed as the feedback law because at each step, A_{k-1} is “fed back” to establish the subsequent value of β_k . For sufficiently

small Δt , this procedure ensures that the cost function $J_k = \langle \Psi_k | H_p | \Psi_k \rangle$ monotonically decreases with respect to layer k , i.e., $J_1 \geq J_2 \geq \dots \geq J_l$, following a discretized version of Eq. (C3). It is important to note that a positive limit for Δt ensuring the maintenance of this property can be obtained based on the steps described in Appendix A of [23], and is expressed in terms of the spectral norms of H_p and H_d as

$$\Delta t \leq \frac{1}{4 \|H_p\| \|H_d\|^2}. \quad (8)$$

In each step k of an FQA implementation, the quantum state $|\Psi_k\rangle$ is prepared by applying the k -layer quantum circuit $U_k(\beta_k) U_p \dots U_d(\beta_1) U_p$ to the fixed initial state $|\Psi_0\rangle$. At the end of this circuit, the value of A_k can be estimated, for example, through repeated measurements of the observable $i[H_d, H_p]$, decomposed into a linear combination of Pauli operators, in the state $|\Psi_k\rangle$.

IV. RESULTS

In this section, we show how a quantum computer can be used to study complex magnetic systems using FALQON. This section is divided into four subsections. First, we demonstrate how to use FALQON to calculate the ground and excited states. Following this, we illustrate how this tool can be employed to study quan-

tum phase transitions, spin correlation functions, and the magnetic structure factor.

A. Calculating Ground and Excited State Energies Using FALQON

To use FALQON as a tool to study magnetic systems, we first define the Hamiltonian H_d as:

$$H_d = \sum_{j=1}^L \sigma_j^x. \quad (9)$$

This is the standard way the mixer is defined in the literature. Although it is not strictly necessary to define it this way, we adhere to this convention in our work. Figure 3 shows the numerical simulations of FALQON applied to the ANNNI model for chains of 3 to 12 sites, with different values of κ and g . The simulations use $\Delta t = 0.02$. Each panel illustrates the convergence of the cost function, $J = \langle \Psi_k | H_p | \Psi_k \rangle$, as a function of the number of layers, for different chain lengths. The expected value of the objective function monotonically decreases with the number of layers, demonstrating the convergence of FALQON to the ground state, even for values close to the transition lines where quantum fluctuations are more intense.

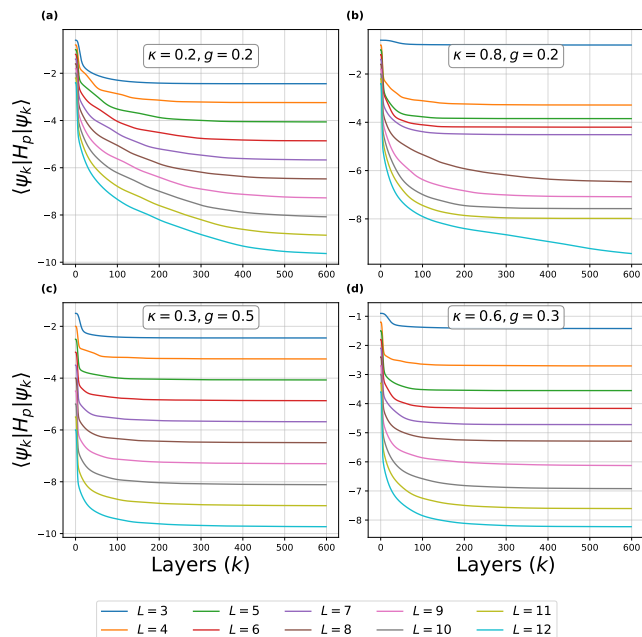


Figure 3. Numerical simulations of FALQON applied to the ANNNI model for chains of 3 to 12 sites with different values of κ and g . Simulations use $\Delta t = 0.02$. In the panels, the curves show the convergence of the cost function, $J = \langle \Psi_k | H_p | \Psi_k \rangle$, as a function of layer k , when qubits are initialized in the ground state of H_d .

It is worth noting that the value of Δt is directly re-

lated to the chain size L , and an appropriate choice results in satisfactory performance. Good performance can be achieved in practice for Δt values significantly exceeding the limit presented in Eq. (8). However, when Δt is too large, we observe that the algorithm does not converge. In this regime, the parameters β_k oscillate drastically, and the objective function does not decrease monotonically (for more details, see [1]). In practice, FALQON does not require evaluations of the objective function at every step; it only needs the estimation of A_k to define each β_k value. Thus, signs of oscillatory behavior in β_k (or equivalently, in the record of A_k measurements) may indicate that Δt is too large and the algorithm is not converging.

In addition to the ground state, it is also possible to use FALQON to calculate the energy of the excited states. We demonstrate that this can be achieved by considering the symmetry of the initial state in the FALQON algorithm. We have found that, depending on the initial conditions, if the initial state shares the same symmetry as the excited states of the Hamiltonian, the algorithm converges to these excited states rather than the ground state. This is significant because we aim to calculate the energy of the excited states. The idea is to first determine the symmetry of the excited states, which can be done using a small lattice, and then initialize the algorithm with a state that has this symmetry. This enables us to calculate the energy of the excited states for systems with many qubits, providing a method to study different properties of magnetic systems.

To account for different symmetries, we investigate the convergence of FALQON under various initial conditions, each corresponding to a different eigenstate of H_d and characterized by specific quantum numbers. Each state is identified by the following expression:

$$|\chi_i, p_I, p_R, p_{T^2}, p_T\rangle \quad (10)$$

where χ_i represents the i -th lowest energy eigenstate of the Hamiltonian H_d , and p_I , p_R , p_{T^2} , and p_T are the corresponding quantum numbers for inversion, reflection, translation squared, and translation, respectively, which are explained in Appendix A.

Some initial states may not have certain quantum numbers; in such cases, we use the symbol $(-)$ in the corresponding position for that quantum number. For example, $|\chi_1, 1, 1, 1, -\rangle$ denotes the first excited state of H_d with $p_I = 1$, $p_R = 1$, $p_{T^2} = 1$, and $p_T = -$ indicating that this state is not an eigenstate of the translation operator. Figure 4 presents the convergence results for parameters $\kappa = 0.2, g = 0.2$ (Figure 4(a)), $\kappa = 0.8, g = 0.2$ (Figure 4(b)), and $\kappa = 0.5, g = 0.8$ (Figure 4(c)), corresponding to different phases of the model. In Figures 4(a, b, c), the state $|\chi_0, 0, 0, 0, 0\rangle$ reaches the ground state of the Hamiltonian, while the state $|\chi_1, 1, 0, 0, 0\rangle$ reaches the first excited state in (a), and $|\chi_1, 1, 1, 1, -\rangle$ in (b, c). It is worth noting that, as shown in Table I in Appendix A, the initial states possess the same symmetries as the

states they converge to. With these results, we are now ready to begin the analysis of the ANNNI model.

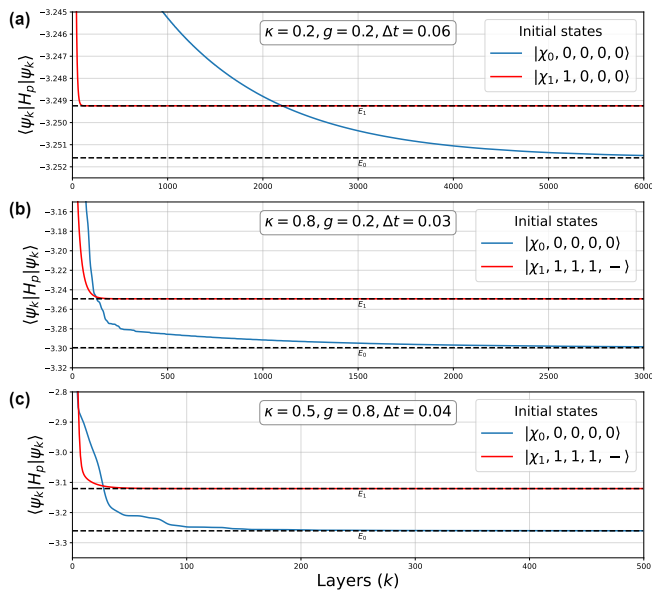


Figure 4. Numerical simulations of FALQON applied to the ANNNI model for a chain with 4 sites, for parameters $\kappa = 0.2, g = 0.2$ (a), $\kappa = 0.8, g = 0.2$ (b), and $\kappa = 0.5$ and $g = 0.8$ (c). In the figures, dashed lines indicate the energy levels of the ANNNI Hamiltonian, while curves represent the convergence of the cost function $J = \langle \Psi_k | H_p | \Psi_k \rangle$ as a function of layer k , when qubits are initialized in different eigenstates of H_x .

B. Quantum Phase Transition

Since we have presented a strategy to calculate the energy of the ground and excited states of the ANNNI model, we can now explore various properties of the model. We begin by examining the quantum phase transitions. For this purpose, we used the Finite Size Scaling method to detect the phase transition (for more details, see Appendix B). Through FALQON, we calculated the energy gap between the ground state and the first excited state by varying the chain sizes. For fixed values of g , the parameter κ was varied, presenting the energy gap ΔE as a function of κ . From the intersection between two adjacent chain sizes, L and $L + 1$, we performed a linear extrapolation to $\frac{1}{L} \rightarrow 0$. Figure 5(a) depicts the relationship between the energy gap of the first excited state with respect to the ground state ($\Delta E \cdot L$) and the next-nearest-neighbor parameter (κ) for different chain sizes, with the external field parameter g fixed at 0.4. To obtain the first excited state, considering these crossings occur in the ferromagnetic phase, we initialize FALQON with the state $|\chi_1, 1, 0, 0, 0\rangle$.

The behavior of energy gap crossings as a function of the parameter κ provides crucial insights into the phase

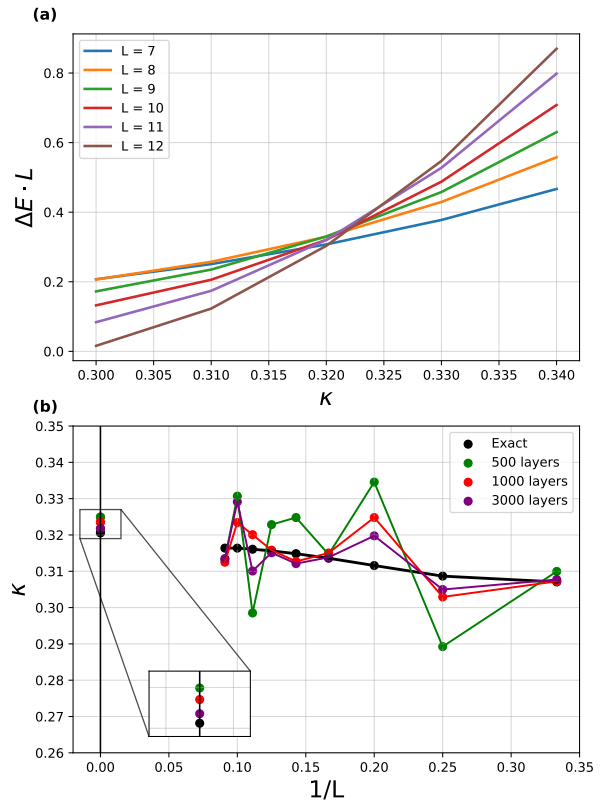


Figure 5. Application of the Finite Size Scaling method using FALQON. In (a), the energy gap ΔE is presented as a function of κ for various finite lattices near the critical region, with $g = 0.40$ and 3000 layers of FALQON. In (b), the Finite-Size dependence of the parameter κ as a function of $\frac{1}{L}$ is shown, as obtained in (a), for different layers of FALQON, compared with the exact value. Each point represents the intersection between two adjacent chain sizes, L and $L + 1$, where a linear extrapolation to $\frac{1}{L} = 0$ is performed.

transition of the system under study. Finite Size Scaling (FSS) method is used to extrapolate these crossings, allowing estimation of the critical point of the phase transition. As $\frac{1}{L}$ tends to zero, the crossings converge to the critical point, marking the phase transition point, as illustrated in Figure 5(b), which shows the relationship between the parameter κ and $\frac{1}{L}$. The data are plotted for different numbers of FALQON layers: 500 layers, 1000 layers, and 3000 layers, compared against the exact value. Extrapolation to $\frac{1}{L} \rightarrow 0$ is crucial for determining the critical point of the phase transition. The convergence point of the crossings from different datasets provides a reliable estimate of the system's critical point.

The combined analysis of Figure 5(a) and the extrapolation in Figure 5(b) reinforces the effectiveness of FSS method as a robust tool for identifying and characteriz-

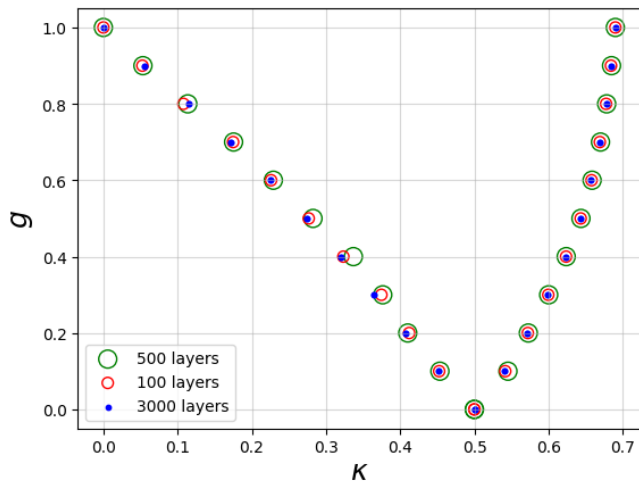


Figure 6. Global phase diagram obtained through FALQON.

ing phase transitions in various systems. This approach allows for accurate estimation of the critical point of the phase transition.

Figure 6 shows the phase diagram obtained with the current approach using FALQON. For $\kappa < 0.5$, the methodology illustrated in Figure 5 was employed. However, the method described above is capable only of characterizing second-order transitions. Transitions between floating phases, i.e., for $\kappa > 0.5$, are challenging to obtain within the current scheme, mainly because we can only use finite systems, which restricts the possible number of states with different modulations in these phases. Nonetheless, a finite-size estimate for first-order transitions can be obtained by calculating points for a fixed size network.

To identify the transition line for $\kappa > 0.5$, we conducted an analysis of points at which the first excited state changes its quantum number, indicating a phase configuration change. We initialized FALQON with two different states: $|\chi_1, 1, -, 1, 7\rangle$ and $|\chi_1, 1, 1, 0, -\rangle$. The first state converges to the first excited state of H_p in the paramagnetic phase in an 8-site chain, while the second state converges to the first excited state in the antiphase. Keeping g values constant, we varied the parameter κ to find the point at which the two states converged to the same expected energy value, indicating the crossing point and hence the phase transition.

C. Correlation Functions

In this section, we used the ground state obtained with FALQON to calculate the correlation functions, considering different values of κ and g that represent various phases of the model. Figure 7 shows the spin correlation functions in real space according to Eq. (B2), calculated using the ground state obtained through FALQON for a 12-site chain ($L = 12$), varying the number of algorithm

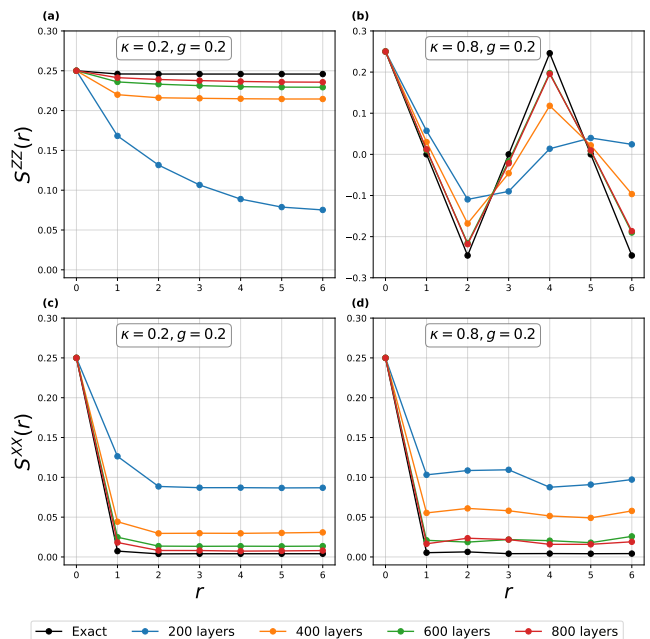


Figure 7. Real-space spin correlation functions of the ANNNI model for an 12-site chain, varying the number of layers of FALQON, for different values of κ and g . The simulations use $\Delta t = 0.02$. In (a) and (b), spatial dependence of the zz correlation function, (a) $\kappa = 0.2, g = 0.2$, and (b) $\kappa = 0.8, g = 0.2$. In (c) and (d), spatial dependence of the xx correlation function, (c) $\kappa = 0.2, g = 0.2$, and (d) $\kappa = 0.8, g = 0.2$.

layers and comparing with exact diagonalization. In Figure 7 (a, b), we have the spin correlation function $S^{zz}(r)$ calculated for parameters (a) $\kappa = 0.2, g = 0.2$ and (b) $\kappa = 0.8, g = 0.2$. In Figure 7 (c, d), we have the spin correlation function $S^{xx}(r)$ calculated for parameters (c) $\kappa = 0.2, g = 0.2$ and (d) $\kappa = 0.8, g = 0.2$. It can be observed that as we increase the number of layers, the correlation function approaches the exact value.

Spin correlation functions provide crucial information about how spins are correlated at different positions along the chain. They describe the probability of finding two spins along the chain with specific orientations at a given separation r . To understand the magnetic properties, it is essential to analyze the behavior of correlations in different magnetic phases of the system. Distinct changes in these characteristics can indicate magnetic phase transitions, where the system transitions from one magnetic configuration to another. The analysis of spin correlation functions in real space allows not only to identify magnetic phases but also to understand the long-range properties and magnetic order present in the system.

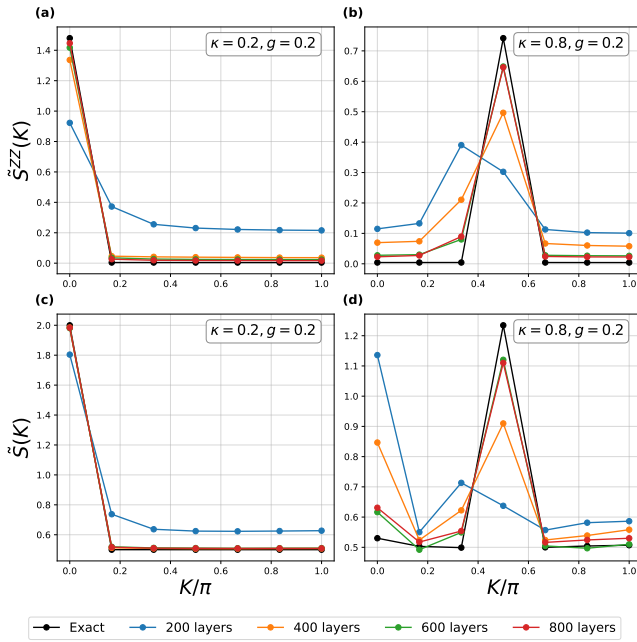


Figure 8. Magnetic structure factors of the ANNNI model for an 12-site chain, varying the number of layers of FALQON, for different values of κ and g . The simulations use $\Delta t = 0.02$. In (a) and (b), magnetic structure factor $\tilde{S}^{zz}(K)$, (a) $\kappa = 0.2$, $g = 0.2$, and (b) $\kappa = 0.8$, $g = 0.2$. In (c) and (d), the sum of the magnetic structure factors. In (c) $\kappa = 0.2$, $g = 0.2$, and in (d) $\kappa = 0.8$, $g = 0.2$.

D. Magnetic Structure Factors

Finally, we studied the magnetic structure factors and their sums. Using the ground state and Equations (B3, B4), we calculated the structure factors and their sums for $K = 0, \dots, L$ (see Appendix B). The magnetic structure factors in Figure 8 provide a description of the spatial distribution of magnetic correlations along the one-dimensional chain, calculated for a 12-site chain with varying layers of the FALQON algorithm. In Figure 8 (a, b), we have the factor $\tilde{S}^{zz}(K)$ calculated for the parameters (a) $\kappa = 0.2$; $g = 0.2$ and (b) $\kappa = 0.8$; $g = 0.2$. In Figure 8 (c, d), we have the sum of the factors $\tilde{S}(K)$ calculated for the parameters (c) $\kappa = 0.2$; $g = 0.2$ and (d) $\kappa = 0.8$; $g = 0.2$.

The magnetic structure factors $\tilde{S}^{\mu\mu}(K)$ provide information about how spins at different positions along the chain are correlated, with different K revealing different length scales relevant to the magnetic properties of the system. Meanwhile, the sum of the magnetic structure factors provides an aggregate view of the global magnetic properties of the system, highlighting aspects common to all spin directions, crucial for understanding magnetic order patterns that may arise in the model's ground state. By studying the dependencies of $\tilde{S}(K)$ on K , significant variations can be identified, indicating different magnetic characteristics of the system. For example, peaks may

suggest specific oscillation modes or magnetic orders, while valleys may indicate regions where magnetic correlation is weaker.

The magnetic structure factors and their sums are crucial tools for characterizing the magnetic properties of models such as the ANNNI model. Through the analysis of these quantities, valuable insights can be gained into the local and global magnetic behavior of the system in its ground state, revealing information about magnetic phases and phase transitions that the system may undergo.

V. CONCLUSION

In this work, we explored the potential of a feedback-based quantum algorithm to analyze the critical properties of the ANNNI model. Our approach successfully computed both ground and excited states without classical optimization methods, highlighting the efficiency of the FALQON algorithm. We studied how FALQON responds when initialized with different eigenstates of H_x , utilizing the symmetries present in the ANNNI model, including inversion, reflection, and translation. By initializing with different eigenstates, we demonstrated that the algorithm allows us to reach excited states by starting from initial states that share their symmetries, thus enabling us to calculate the energy of these higher energy configurations.

Our detailed exploration included the phase diagram, correlation functions, and structure factors. We employed the Finite Size Scaling method to study quantum phase transitions, analyzed spin correlations in the ground state to understand correlation functions, and used the Discrete Fourier Transform to examine magnetic structure factors. Our findings establish FALQON as a powerful tool to study magnetic systems, offering valuable insights into the magnetic behavior and critical properties of the ANNNI model. Future research may extend this approach to other quantum systems, further validating the robustness and versatility of feedback-based quantum algorithms in studying many-body quantum phenomena.

ACKNOWLEDGMENTS

F.F.F acknowledge support from Fundação de Amparo à Pesquisa do Estado de São Paulo (FAPESP), project number 2023/04987-6 and from ONR, project number N62909-24-1-2012. G. E. L. P. and L. A. M. R. thank the support provided by the Conselho Nacional de Desenvolvimento Científico (CNPQ).

Appendix A: Symmetries

The analysis of the one-dimensional ANNNI model with a transverse field is facilitated by investigating its symmetries. A symmetry is a transformation that, when applied to a physical system, does not alter its observable properties, making it invariant under this transformation.

Consider an operator P representing a transformation acting on a chain of L spin-1/2 sites. If this transformation is a symmetry of the system, then P commutes with the system's Hamiltonian H ($[P, H] = 0$). This implies that all subspaces of P are invariant under the action of H [24], allowing the construction of a set of eigenvectors common to both H and P . The eigenvectors of H can be identified by the eigenvalues ϕ_p of P , providing an additional identification to the eigenstates of H beyond their energy E_h . For simplicity, we refer to the eigenvalue ϕ_p simply as p , which will be the quantum number associated with P .

If the system has more than one symmetry $\{P_1, P_2, \dots, P_n\}$ and the operators representing them commute with each other, it is possible to construct a basis from the eigenvectors common to H and these operators. In this basis, the representation of the Hamiltonian matrix takes a block-diagonal form [25], where each block corresponds to a vector subspace characterized by the quantum numbers p_1, p_2, \dots, p_n . This subspace is referred to as the sector of quantum numbers p_1, p_2, \dots, p_n . The vectors belonging to these subspaces are eigenvectors of the operators, represented by:

$$|h, p_1, p_2, \dots, p_n\rangle. \quad (\text{A1})$$

The invariance of P under the action of H also extends to the temporal evolution of the system. If a system is in an eigenstate of P at an initial time t_0 , it will remain in that eigenstate with the same eigenvalue until a later time t [26]. This is represented by the equation:

$$PU(t, t_0)|p\rangle = U(t, t_0)P|p\rangle = \phi_p U(t, t_0)|p\rangle \quad (\text{A2})$$

where $U(t, t_0)$ is the time evolution operator from t_0 to t . Thus, if at time t_0 , the system is in a state belonging to a specific sector of quantum numbers, then after the temporal evolution up to time t , the state of the system will continue to belong to the same sector.

If P is a cyclic symmetry of order n (\mathbb{Z}_n) [27], meaning it has a period n , where applying P n times to a specific state results in the same initial state:

$$P^n|\psi\rangle = |\psi\rangle \quad (\text{A3})$$

where $|\psi\rangle$ is any state. Then the eigenvectors of P can be expressed as:

$$|p\rangle = C \sum_{j=0}^{r-1} (\phi_p P)^j |\psi\rangle \quad (\text{A4})$$

where C is a normalization constant. The eigenvalues of P are expressed as:

$$\phi_p = e^{i\frac{2\pi}{L}p}, \quad p = 0, 1, \dots, n-1 \quad (\text{A5})$$

If $|p\rangle = 0$, then it is not possible to form an eigenvector of P with eigenvalue ϕ_p from the state $|\psi\rangle$. In the ANNNI model, three main symmetries are identified: spin inversion, spatial reflection, and translation. The spin inversion symmetry, represented by the operator I , acts on a state by flipping the spins at each site:

$$|++-+-++\rangle \rightarrow |--+--+--\rangle.$$

Being a cyclic symmetry of order two, it has eigenvalues $\phi_{p_I} = \pm 1$, with corresponding eigenvectors:

$$|j, p_I\rangle = C[\mathbb{1} + \phi_{p_I} I]|\psi\rangle \quad (\text{A6})$$

where C is a normalization constant and j is a degeneracy index.

The reflection symmetry is represented by the operator R and flips the spin order about a central reflection point in the chain:

$$R|d_0 d_1 \dots d_{L-2} d_{L-1}\rangle = |d_{L-1} d_{L-2} \dots d_1 d_0\rangle.$$

Similar to I , R is a cyclic symmetry of order two. Its eigenvalues are $\phi_{p_R} = \pm 1$, with corresponding eigenvectors:

$$|j, p_R\rangle = C[\mathbb{1} + \phi_{p_R} R]|d_0 d_1 d_2 \dots d_{L-1}\rangle. \quad (\text{A7})$$

The translation symmetry is represented by the operator T . When acting on the chain, it shifts the site positions cyclically:

$$T|d_0 d_1 \dots d_{L-2} d_{L-1}\rangle = |d_1 d_2 \dots d_{L-1} d_0\rangle. \quad (\text{A8})$$

T is a cyclic symmetry with an order equal to the chain size. Its eigenvalues are $\phi_{p_T} = e^{i\frac{2\pi}{L}p_T}$, where $p_T = 0, 1, \dots, L-1$. The corresponding eigenvectors are:

$$|j, p_T\rangle = C[\mathbb{1} + \phi_{p_T} T + \dots + (\phi_{p_T} T)^{L-1}]|\psi\rangle. \quad (\text{A9})$$

We could use the operators I, R , and T to form a set of commuting operators. However, this is not possible because the reflection operator R does not commute with the translation operator T for all chain sizes. To resolve this issue, we can instead use one of the powers of T in place of T directly. In chains with an even number of sites, we can use the operator $T^{L/2}$ as a substitute, which has eigenvalues $\phi_{p_{T^{L/2}}} = \pm 1$ with eigenvectors:

$$|j, p_{T^{L/2}}\rangle = C[\mathbb{1} + \phi_{p_{T^{L/2}}} T^{L/2}]|\psi\rangle. \quad (\text{A10})$$

This way, we can identify the eigenvectors of the

Hamiltonian by the quantum numbers $h, p_I, p_R, p_{T^{L/2}}$:

$$|h, p_I, p_R, p_{T^{L/2}}\rangle. \quad (\text{A11})$$

In some sectors of the system, the translation operator commutes with the inversion and reflection operators. In these cases, the sectors can be further subdivided into smaller sectors, also characterized by p_T . Thus, by constructing a common basis for the operators $I, R, T^{L/2}$ through successive applications of Eqs. (A6, A8, A10), we can obtain a block-diagonal representation for the Hamiltonian of the ANNNI model. Table I presents the spectrum of the Hamiltonian of the ANNNI model for a chain of 4 sites, obtained through exact diagonalization of each block of the block-diagonal representation. Two distinct parameter sets are considered: $\kappa = 0.2, g = 0.2$ and $\kappa = 0.8, g = 0.2$. Each row in the table represents a specific configuration of quantum numbers characterizing the sector, along with the energies of the eigenstates associated with these configurations for the two parameter sets.

Table I. Spectrum of the Hamiltonian of the ANNNI model for a 4-site chain, with different parameter sets (κ and g). The quantum numbers p_I, p_R, p_{T^2} , and p_T indicate inversion, reflection, translation squared, and translation transformations, respectively. The energies of the eigenstates associated with these configurations are shown for the two parameter sets. When a quantum number is not present, it is represented by "-", indicating the absence of that transformation for the corresponding state.

p_I	p_R	p_{T^2}	p_T	$E(\kappa = 0.2, g = 0.2)$	$E(\kappa = 0.8, g = 0.2)$
0	0	0	0	-3.2516	-3.2994
0	0	0	0	-1.0829	-0.9493
0	0	0	2	-0.8000	-3.2000
0	0	0	0	0.3008	0.2263
0	0	0	0	4.8336	7.2223
1	0	0	0	-3.2492	-0.9657
1	0	0	0	0.0492	0.1657
0	1	0	2	0.0000	0.0000
1	1	0	2	-0.0331	-0.0222
1	1	0	2	4.8331	7.2222
0	0	1	-	0.0000	0.0000
1	0	1	-	-0.9657	-3.2492
1	0	1	-	0.1657	0.0492
0	1	1	-	0.0000	0.0000
1	1	1	-	-0.9657	-3.2492
1	1	1	-	0.1657	0.0492

Appendix B: Finite Size Scaling and Magnetic Properties

The Finite Size Scaling (FSS) method, introduced by Fisher and Barber [28, 29], is a powerful tool in statistical physics and the theory of critical systems. It is often used

to study the behavior of physical systems around critical points in finite dimensions, especially in systems with phase transitions. The fundamental idea behind FSS is that the physical properties of a system depend on its size in a predictable and universal manner.

The energy gap of the quantum Hamiltonian $\Delta(\kappa, g)$ as a function of parameters (κ, g) is inversely proportional to the correlation length ξ . Thus, in the thermodynamic limit, as the chain size $L \rightarrow \infty$, the energy gap tends to zero at the critical point, $\Delta(\kappa, g) \rightarrow 0$, leading to a singularity where the correlation length diverges, $\xi \rightarrow \infty$. At the transition point, we have $\xi \approx L$, so that we obtain

$$\frac{L}{\xi} = L \cdot \Delta(\kappa, g) = L \cdot (E_1(\kappa, g) - E_0(\kappa, g)) \rightarrow 1, \quad (\text{B1})$$

where $E_0(\kappa, g)$ is the ground state energy and $E_1(\kappa, g)$ is the energy of the first excited state calculated at point (κ, g) for a chain of L sites. An estimate for the critical point (phase transition point) can be obtained when the function $L \cdot (E_1(\kappa, g) - E_0(\kappa, g))$ coincides for two adjacent chain sizes, L and $L + 1$. In practical terms, we plot the function $L \cdot (E_1(\kappa, g) - E_0(\kappa, g))$ while fixing one parameter and varying the other. When the plots for two adjacent chain sizes overlap, the intersection point of these curves provides the estimate of the critical point. By repeating this process for successive pairs of larger chains, we obtain a sequence of estimates that converge to the value of the critical point as $L \rightarrow \infty$.

To investigate the magnetic properties obtainable exclusively from the ground state in the context of the ANNNI model, our aim was to explore the intricate relationships of the correlation functions that emerge, highlighting the nuances and implications these correlations have on the magnetic properties of the system.

Understanding the ground state allows us to compute the magnetic properties associated with each of the magnetic phases of the system, characterized by spin correlation functions in real space,

$$S^{\mu\mu}(r) = \langle S_i^\mu S_{i+r}^\mu \rangle, \quad \mu = x, y, z, \quad (\text{B2})$$

and their corresponding magnetic structure factors via the Discrete Fourier Transform,

$$\tilde{S}^{\mu\mu}(K) = \frac{1}{L} \sum_{i,j=1}^L e^{iK(i-j)} \langle S_i^\mu S_j^\mu \rangle, \quad \mu = x, y, z, \quad (\text{B3})$$

as well as their sums,

$$\tilde{S}(K) = \sum_{\mu=x,y,z} \tilde{S}^{\mu\mu}(K), \quad (\text{B4})$$

where $\langle \dots \rangle \equiv \langle \psi_0 | \dots | \psi_0 \rangle$ denotes the average value in the ground state, $S_i^\mu = \frac{1}{2} \sigma_i^\mu$ is the spin operator component at site i (assuming $\hbar = 1$), r is the distance between the sites where the correlation is being measured, and K

(in units of $2\pi/L$) is the wave number characterizing the periodicity of magnetic ordering.

Appendix C: Quantum Lyapunov Control

The quantum Lyapunov control framework is utilized to design one or more time-dependent controls aiming to asymptotically guide a quantum dynamical system towards a desired state [30]. To introduce this framework, we start with a quantum system governed by the time-dependent Schrödinger equation (assuming $\hbar = 1$),

$$i\frac{d}{dt}|\Psi(t)\rangle = [H_p + H_d\beta(t)]|\Psi(t)\rangle, \quad (\text{C1})$$

where H_p represents the time-independent part of the Hamiltonian, referred to as the problem Hamiltonian. On the other hand, H_d denotes the control Hamiltonian, which couples a time-dependent control function $\beta(t)$ to the system; this is termed the driver Hamiltonian. The extension to cases with multiple control functions is straightforward, as discussed, for example, in Ref. [16].

The quantum control problem addresses the projection of $\beta(t)$ to guide $|\Psi(t)\rangle$ towards a state that minimizes an objective function J . Quantum Lyapunov control has been developed for various distinct objective functions, such as capturing the distance to a target state [31–33], the error relative to the target state [34], and the expected value of a target observable. In this context, we focus on the observable case and define J as the expected value of H_p ,

$$J = \langle \Psi(t) | H_p | \Psi(t) \rangle. \quad (\text{C2})$$

To solve the control problem, the Lyapunov control method seeks a function $\beta(t)$ that leads to a monotonically decreasing objective function J over time t . This method is asymptotic, eliminating the need to specify an

endpoint in advance. Particularly, we seek a $\beta(t)$ function that satisfies the derivative condition:

$$\frac{dJ}{dt} \leq 0, \forall t. \quad (\text{C3})$$

Evaluating the left-hand side of Eq. (C3) using Eqs. (C1) and (C2), we obtain:

$$\frac{dJ}{dt} = A(t)\beta(t), \quad (\text{C4})$$

where $A(t)$ abbreviates the time-dependent expectation value $A(t) \equiv \langle \Psi(t) | i[H_d, H_p] | \Psi(t) \rangle$. The derivative condition in Eq. (C3) can be satisfied by choosing $\beta(t) = wf(t, A(t))$, where $w > 0$ is a positive weight and $f(t, A(t))$ is chosen such that $f(t, 0) = 0$ and $A(t)f(t, A(t)) > 0$ for all $A(t) \neq 0$. The specific formulation used in this article considers $w = 1$ and $f(t, A(t)) = A(t)$, resulting in the following control law:

$$\beta(t) = -A(t). \quad (\text{C5})$$

This control law satisfies the condition set by Eq. (C3), resulting in $\frac{dJ}{dt} = -(A(t))^2 \leq 0$ for all $A(t)$.

The convergence of quantum Lyapunov control has been analyzed using the LaSalle’s invariance principle [35], which identified a set of sufficient conditions to ensure asymptotic convergence to the global minimum of Eq. (C2). However, these conditions are often stringent and rarely met in practical applications. Nonetheless, convergence to the global minimum is frequently observed in practice, as demonstrated by numerical simulations [1, 15], even in scenarios where theoretical convergence criteria are not satisfied. Better understanding the necessary conditions for the convergence of quantum Lyapunov control, in order to bridge the gap between mathematical results and numerical observations, remains an open and intriguing research challenge.

-
- [1] J. B. Larsen, M. D. Grace, A. D. Baczewski, and A. B. Magann, Feedback-based quantum algorithms for ground state preparation (2023), [arXiv:2303.02917](https://arxiv.org/abs/2303.02917).
- [2] D. Poulin and P. Wocjan, Preparing ground states of quantum many-body systems on a quantum computer, *Physical Review Letters* **102**, [10.1103/PhysRevLett.102.130503](https://doi.org/10.1103/PhysRevLett.102.130503) (2009).
- [3] N. M. Tubman, C. Mejuto-Zaera, J. M. Epstein, D. Hait, D. S. Levine, W. Huggins, Z. Jiang, J. R. McClean, R. Babbush, M. Head-Gordon, and K. B. Whaley, Postponing the orthogonality catastrophe: efficient state preparation for electronic structure simulations on quantum devices (2018), [arXiv:1809.05523](https://arxiv.org/abs/1809.05523) [quant-ph].
- [4] Y. Ge, J. Tura, and J. I. Cirac, Faster ground state preparation and high-precision ground energy estimation with fewer qubits (2018), [arXiv:1712.03193](https://arxiv.org/abs/1712.03193) [quant-ph].
- [5] L. Lin and Y. Tong, Near-optimal ground state preparation, *Quantum* **4**, 372 (2020).
- [6] J. Kempe, A. Kitaev, and O. Regev, The complexity of the local hamiltonian problem (2005), [arXiv:quant-ph/0406180](https://arxiv.org/abs/quant-ph/0406180) [quant-ph].
- [7] J. Preskill, Quantum computing in the NISQ era and beyond, *Quantum* **2**, 79 (2018).
- [8] M. Cerezo, A. Arrasmith, R. Babbush, S. C. Benjamin, S. Endo, K. Fujii, J. R. McClean, K. Mitarai, X. Yuan, L. Cincio, and P. J. Coles, Variational quantum algorithms, *Nature Reviews Physics* **3**, 625 (2021).
- [9] K. Bharti, A. Cervera-Lierta, T. H. Kyaw, T. Haug, S. Alperin-Lea, A. Anand, M. Degroote, H. Heimonen, J. S. Kottmann, T. Menke, W.-K. Mok, S. Sim, L.-C. Kwek, and A. Aspuru-Guzik, Noisy intermediate-scale quantum algorithms, *Reviews of Modern Physics* **94**, [10.1103/revmodphys.94.015004](https://doi.org/10.1103/revmodphys.94.015004) (2022).
- [10] A. Peruzzo, J. McClean, P. Shadbolt, M.-H. Yung, X.-Q.

- Zhou, P. J. Love, A. Aspuru-Guzik, and J. L. O'Brien, A variational eigenvalue solver on a photonic quantum processor, *Nature Communications* **5**, [10.1038/ncomms5213](https://doi.org/10.1038/ncomms5213) (2014).
- [11] J. Tilly, H. Chen, S. Cao, D. Picozzi, K. Setia, Y. Li, E. Grant, L. Wossnig, I. Rungger, G. H. Booth, and J. Tennyson, The variational quantum eigensolver: A review of methods and best practices, *Physics Reports* **986**, 1–128 (2022).
- [12] A. Kandala, A. Mezzacapo, K. Temme, and et al., Hardware-efficient variational quantum eigensolver for small molecules and quantum magnets, *Nature* **549**, 242 (2017).
- [13] E. Farhi, J. Goldstone, and S. Gutmann, A quantum approximate optimization algorithm, arXiv preprint arXiv:1411.4028 (2014).
- [14] S. Cong and F. Meng, A survey of quantum lyapunov control methods, *The Scientific World Journal* **2013**, 1 (2013).
- [15] A. B. Magann, K. M. Rudinger, M. D. Grace, and M. Sarovar, Feedback-based quantum optimization, *Physical Review Letters* **129**, [10.1103/physrevlett.129.250502](https://doi.org/10.1103/physrevlett.129.250502) (2022).
- [16] A. B. Magann, K. M. Rudinger, M. D. Grace, and M. Sarovar, Lyapunov-control-inspired strategies for quantum combinatorial optimization, *Physical Review A* **106**, [10.1103/physreva.106.062414](https://doi.org/10.1103/physreva.106.062414) (2022).
- [17] M. E. Fisher and W. Selke, Infinitely many commensurate phases in a simple ising model, *Phys. Rev. Lett.* **44**, 1502 (1980).
- [18] W. Selke, The annni model — theoretical analysis and experimental application, *Physics Reports* **170**, 213 (1988).
- [19] A. K. Chandra and S. Dasgupta, Floating phase in the one-dimensional transverse axial next-nearest-neighbor ising model, *Phys. Rev. E* **75**, 021105 (2007).
- [20] A. J. Ferreira-Martins, L. Silva, A. Palhares, R. Pereira, D. O. Soares-Pinto, R. Chaves, and A. Canabarro, Detecting quantum phase transitions in a frustrated spin chain via transfer learning of a quantum classifier algorithm (2023), [arXiv:2309.15339](https://arxiv.org/abs/2309.15339) [quant-ph].
- [21] M. Cea, M. Grossi, S. Monaco, E. Rico, L. Tagliacozzo, and S. Vallecorsa, Exploring the phase diagram of the quantum one-dimensional annni model (2024), [arXiv:2402.11022](https://arxiv.org/abs/2402.11022) [cond-mat.str-el].
- [22] Y.-T. Yang and H.-G. Luo, Pattern description of the ground state properties of the one-dimensional axial next-nearest-neighbor ising model in a transverse field (2023), [arXiv:2301.08891](https://arxiv.org/abs/2301.08891) [cond-mat.stat-mech].
- [23] A. B. Magann, S. E. Economou, and C. Arenz, Randomized adaptive quantum state preparation, *Physical Review Research* **5**, [10.1103/physrevresearch.5.033227](https://doi.org/10.1103/physrevresearch.5.033227) (2023).
- [24] C. Cohen-Tannoudji, B. Diu, and F. Laloe, Quantum mechanics, volume 1, *Quantum Mechanics* **1** (1986).
- [25] J.-H. Jung and J. D. Noh, Guide to exact diagonalization study of quantum thermalization, *Journal of the Korean Physical Society* **76**, 670–683 (2020).
- [26] J. J. Sakurai and J. Napolitano, *Modern Quantum Mechanics*, 3rd ed. (Cambridge University Press, 2020).
- [27] Y.-H. Lin and S.-H. Shao, z_N symmetries, anomalies, and the modular bootstrap, *Phys. Rev. D* **103**, 125001 (2021).
- [28] M. Fisher and M. N. Barber, Scaling theory for finite-size effects in the critical region, *Phys. Rev. Lett.* **28**, 1516 (1972).
- [29] C. J. Hamer and M. N. Barber, Finite-lattice methods in quantum hamiltonian field theory. I. The Ising model, *J. Phys. A: Math* **14** (1981).
- [30] S. C. Hou, M. A. Khan, X. X. Yi, D. Dong, and I. R. Petersen, Optimal lyapunov-based quantum control for quantum systems, *Physical Review A* **86**, [10.1103/physreva.86.022321](https://doi.org/10.1103/physreva.86.022321) (2012).
- [31] S. Kuang and S. Cong, Lyapunov control methods of closed quantum systems, *Automatica* **44**, 98 (2008).
- [32] X. Wang and S. G. Schirmer, Analysis of lyapunov method for control of quantum states, *IEEE Transactions on Automatic Control* **55**, 2259 (2010).
- [33] K. Beauchard, J. M. Coron, M. Mirrahimi, and P. Rouchon, Implicit lyapunov control of finite dimensional schrödinger equations, *Systems & Control Letters* **56**, 388 (2007).
- [34] M. Mirrahimi, P. Rouchon, and G. Turinici, Lyapunov control of bilinear schrödinger equations, *Automatica* **41**, 1987 (2005).
- [35] J. P. L. Salle, *The Stability of Dynamical Systems* (SIAM, 1976).